Nanostructured Poly(styrene-*b*-butadiene-*b*-styrene) (SBS) Membranes for the Separation of Nitrogen from Natural Gas

Maria Giovanna Buonomenna, Giovanni Golemme,* Caterina Maria Tone, Maria Penelope De Santo, Federica Ciuchi, and Enrico Perrotta*

The preparation and characterization of new, tailor-made polymeric membranes using poly(styrene-*b*-butadiene-*b*-styrene) (SBS) triblock copolymers for gas separation are reported. Structural differences in the copolymer membranes, obtained by manipulation of the self-assembly of the block copolymers in solution, are characterized using atomic force microscopy, transmission electron microscopy, and the transport properties of three gases (CO_2, N_2, and CH_4). The CH_4/N_2 ideal selectivity of 7.2, the highest value ever reported for block copolymers, with CH_4 permeability of 41 Barrer, is obtained with a membrane containing the higher amount of polybutadiene (79 wt%) and characterized by a hexagonal array of columnar polystyrene cylinders normal to the membrane surface. Membranes with such a high separation factor are able to ease the exploitation of natural gas with high N_2 content. The CO_2/N_2 ideal selectivity of 50, coupled with a CO_2 permeability of 289 Barrer, makes SBS a good candidate for the preparation of membranes for the post-combustion capture of carbon dioxide.

1. Introduction

The demand for natural gas has steadily increased over the past decade and is expected to increase further. This increased demand will require increased production of gas from the existing proven reserves. A significant proportion of the gas reserves are of low quality due to the presence of nitrogen: in the U.S. fourteen percent of known natural gas reserves contain more than 4% inert nitrogen and, therefore, cannot be sent to the national pipeline without treatment. Today, the only process used on a large scale is cryogenic liquefaction and fractionation. Cryogenic plants are most suited to large gas fields, which allow the high capital cost of the cryogenic plant to be defrayed. Many small nitrogen-contamined gas wells are shut in for lack of a suitable small-scale nitrogen separation technology.[1] In addition to this, much of today's gas production is from large, accessible fields, whereas in the future new production will be increasingly from small, remote, or offshore sources.[2] As a result, a technology able to treat small natural gas streams is needed: one proven technology for this case is membrane separation.[1]

Gas transport through dense polymer membranes can be described by the expression in Equation (1):

$$J = P(p_0 - p_l)/l \quad (1)$$

where J is the volumetric flux expressed as cm^3 STP cm^{-2} s^{-1} (STP is (gas at 1 atm, 0 °C), P is the membrane permeability, l is the membrane thickness, p_0 is the partial pressure of the component of interest on the feed side, and p_l is its partial pressure on the permeate side. The ability of a membrane to separate two gases, for example nitrogen and methane, is measured by the ratio of their permeability, the membrane selectivity $\alpha_{N2/CH4}$, expressed by Equation (2):

$$\alpha_{N_2/CH4} = P_{N_2}/P_{CH_4} \quad (2)$$

The selectivity term $\alpha_{CH4/N2}$ (Equation 3) for a methane-selective membrane is the reciprocal of Equation (2).

$$\alpha_{CH_4/N_2} = P_{CH_4}/P_{N_2} \quad (3)$$

Glassy polymers tend to permeate nitrogen preferentially with a maximum expected selectivity $\alpha_{N2/CH4}$ of ≈2.5. Rubbery polymers will tend to permeate methane preferentially with a maximum expected selectivity $\alpha_{CH4/N2}$ of ≈3.5.[1,2] In Table 1 membrane performance data for a variety of methane and carbon dioxide selective membranes are shown.

On the basis of the data in Table 1, Pebax 2533 has the highest value of CH_4/N_2 selectivity, i.e., 4.2. Pebax is a block-copolymer composed of a "hard" aliphatic polyamide (PA) block (e.g., nylon-6, nylon-12) and of a "soft" amorphous polyether block.[6] The PA blocks provide the mechanical strength and gas transport occurs preferentially through the polyether phase.[7–9] Block copolymers with immiscible soft and rigid blocks, such as Pebax, can form various microphase separated structures.

Dr. M. G. Buonomenna, Dr. G. Golemme
Department of Chemical Engineering and Materials
University of Calabria, and Consorzio INSTM
Via P. Bucci, 87036 Rende, Italy
E-mail: mgbuono@unical.it; ggolemme@unical.it
C. M. Tone, Dr. M. P. De Santo, Dr. F. Ciuchi
IPCF-CNR UOS Cosenza, c/o Physics Department
University of Calabria
via P. Bucci, 87036 Rende, Italy
E. Perrotta
Department of Ecology
University of Calabria
Via P. Bucci 4A, 87036 Rende, Italy

DOI: 10.1002/adfm.201101904

Table 1. Intrinsic permeation properties of widely used polymer membrane materials at 30 °C.

Polymer	Permeability (Barrer)			Selectivity		Ref.
	CO_2	CH_4	N_2	CH_4/N_2	CO_2/N_2	
PDMS	2300	760	230	3.3	10	[1]
Poly(siloctylene siloxane)		360	91	4.0		[3]
Poly(*p*-silphenylene siloxane)		12	3	4.0		[3]
Pebax 1657	73	4.7	1.6	2.88	45	[4]
Pebax 2533	110	20	4.8	4.2	23	[1]
PEO_{1000}-TΦT[a)]	105	5.7	1.9	2.95	54.5	[5]
PEO_{1500}-TΦT[a)]	126	6.9	2.4	2.92	53.2	[5]

[a)]Measurements at 35 °C

The microdomain phase separation of the block copolymers is crucial and needs to be controlled. A block copolymer with improved properties for gas permeation should exhibit the following properties: 1) good phase separation of the hard and soft segments; 2) high content of the CO_2 selective soft segment; 3) low glass transition temperature of the soft segment for a high chain flexibility; and 4) no crystallinity or low melting temperature of the soft phase.[5]

Commercially available block copolymers often have incomplete phase separation due to non-uniformity of the hard segment, leading to large fractions of non-crystallized hard segments within the soft amorphous phase. This restricts the amount of soft CO_2 selective block that can be used (property 2) and reduces the chain flexibility (property 3). A schematic representation of the morphology of a typical commercially available block copolymer is shown in **Figure 1**a.

Varying the nature of the hard and the soft segments, the molecular weight and the content of each block, the mechanical, chemical, and physical properties as well as the gas transport features can be modelled.[10–15]

To improve the performance of the block copolymers based on soft amorphous polyether block and to control the microdomain phase separation, Husken et al.[16] used tetramide hard segments with strongly improved crystallization behavior, resulting in almost complete phase separation and enabling high soft phase concentrations (Figure 1b).[16]

To further improve the membrane gas separation properties Wessling et al.[5] proposed the use of a short monodisperse di-amide hard segment (TΦT) (length ≈ 2 nm) instead of the longer tetra-amide hard segment (length ≈ 4.2 nm) used by Husken et al.[16] The introduction of this type of hard segment led to the incorporation of higher amounts of soft segment (property 2). The resulting morphology is shown in Figure 1b. The transport data of the corresponding membranes PEO_{1000}-TΦT and PEO_{1500}-TΦT are reported in Table 1.

In the present work, two poly(styrene-*b*-butadiene-*b*-styrene) (SBS) triblock copolymers with different styrene content (28 and 21 wt%, SBS28 and SBS21, respectively) have been used for the preparation of nanostructured membranes, in particular for the CH_4/N_2 and the CO_2/N_2 separations. The formation of different well-ordered microphase separation (Figure 1c,d) is induced by varying the preparation conditions of the polymeric films, and the influence of the membrane structure on the gas performance is studied. Membranes with good phase separation, well-defined hard phases, and high content of the soft phase have been obtained and they demonstrate unprecedented separation capabilities for the CH_4/N_2 and the CO_2/N_2 gas pairs.

SBSs are rubbery/glassy block copolymers that can be synthesized by means of living anionic polymerization. Nowadays, commercially available products can be divided into two basic types: type I "thermoplastic elastomer" with 60–80 wt% soft phase fraction and type II "transparent ductile thermoplastic" with about 20–30 wt% butadiene fraction. Kraton, which was introduced by the Shell Oil Company and belongs to type I with polybutadiene as the mobile blocks, is of the rubber kind and is used as a soft touch material. Styroflex from BASF also belongs to type I but has poly(styrene-*co*-butadiene) as the mobile blocks. Type II SBS has high hard phase fraction and stretch strain and can therefore be thermoformed and used for packaging films.[17]

SBS is composed of two polystyrene (PS) hard blocks and one central polybutadiene (PB) soft block (**Figure 2**). In the literature, many studies are focussed on the morphology of SBS films: the variables explored are the rate of evaporation of the solvent and the molecular weight of the polymer.[18–22]

Concerning only the applications of SBS membranes, few examples for both pervaporation (PV) and gas separation (GS) applications are reported. The PV processes reported are the recovery of volatile organic compounds, such as 1,1,1–trichloroethane (TCA) and trichloroethylene (TCE), and the removal of toluene and ethanol from diluted aqueous solutions. The obtained results are compared in terms of selectivity and flux with commercial membranes with particular emphasis on the performance and on the nanostructures.[23–26]

For SBS, only a few reports of the gas permeability data have been published. In an early work, Bazzarelli et al.[27] reported the performance of dense SBS membranes with selectivities of 17.7 and 3.1 for the CO_2/N_2 and CH_4/N_2 gas pairs, respectively; the results

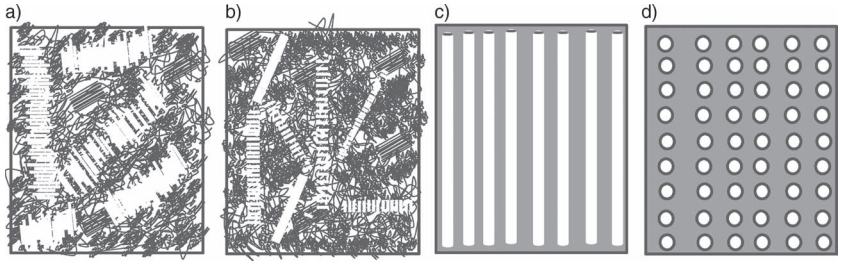

Figure 1. Schematic representation of the morphology of a) commercially available block copolymers (e.g., the PEBAX family), b) polyether-based block copolymers with monodisperse di-amide hard segment (TΦT),[5] and c,d) SBS membranes with hard phase organized in ordered structures (reported here). The grey and white areas are representative for soft and hard phases, respectively.

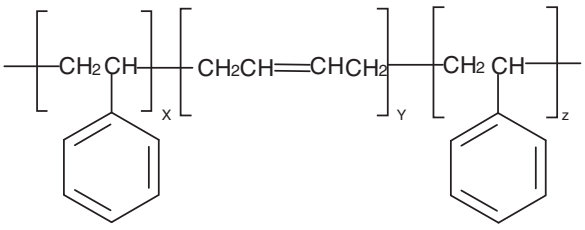

Figure 2. The chemical structure of the SBS triblock copolymers.

improve with SBS composite membranes, for which the best value of CO_2/N_2 selectivity is 36 while the CH_4/N_2 selectivity is 2.6. No information on the membrane nanostructures is given.

Song et al.[28] prepared and characterized films made of SBS (PS 30 wt%) and poly(2,6-dimethyl-1,4-phenylene oxide) (PPO) blends in various proportions to explore their application as gas separation membranes. The selectivities of the blend membrane for the CO_2/N_2 and CH_4/N_2 pairs were 17.9 and 2.2, respectively. The selectivity of the blend membrane increased for the CO_2/N_2 pair with increasing the PPO content up to 23.9 and decreased to 1.98 for the CH_4/N_2 pair.

Kim et al.[29] studied the O_2 and N_2 transport properties of alkylsilane-modified SBS membranes (PS 35 wt%). No information concerning other gases is given. The best result of selectivity for O_2/N_2 pair is 3.2, with 37.5 Barrer and 11.7 Barrer of permeability for O_2 and N_2, respectively.

Peters et al.[30] compared patterned and non-patterned dense membranes based on SBS (PS 29.5 wt%): for both the membrane types they reported the gas permeation data only for He/N_2 (2.50), O_2/N_2 (2.34), and CO_2/N_2 (13.37) pairs. The permeability for CO_2 was 188.4 Barrer.

The purpose of the present work is to relate the nanoscale morphology of the nanostructured membranes with the selective transport of methane and carbon dioxide compared to nitrogen. The nanostructure of SBS membranes has been tuned in solution by changing the solvent used for the membrane preparation at a fixed percentage of PS (21 and 28 wt%). The affinity of the organic solvent in terms of solubility parameters with the hard (PS) and the soft (PB) blocks was the driving force for the organization in different new nanostructures, extensively characterized using atomic force microscopy (AFM) and transmission electron microscopy (TEM). To explain the effect of structural changes in the new copolymer membranes, gas transport properties are discussed.

2. Results and Discussion

2.1. General Considerations

The relative affinity of solvent for each block is measured by the polymer–solvent interaction parameter χ_{PS},

$$\chi_{PS} = V_s(\delta_S - \delta_P)^2 / RT + 0.34 \quad (4)$$

where V_s is the molar volume of the solvent, R is the gas constant, T is the temperature, and δ_S and δ_P are the solubility parameters of the solvent and polymer, which are also convenient to use as a means of estimating the compatibility between the polymer and solvent. For PS and PB the solubility parameters are reported as $\delta_{PS} = 18.6$ $J^{1/2}$ $cm^{-3/2}$ and $\delta_{PB} = 17.0$ $J^{1/2}$ $cm^{-3/2}$, respectively.

Table 2. Polymer-solvent interaction parameters (χ) for different pairs of blocks of SBS polymer (PS and PB) and solvents, calculated according to ref. [31].

	Toluene	Chloroform
PS	0.3469	0.3452
PB	0.4018	0.4704

The calculated polymer–solvent interaction parameters χ for different pairs of blocks of SBS polymers and solvents at room temperature are listed in **Table 2**.

For each solvent, the differences in polymer–solvent interaction parameters between PS and PB concerned with the difference in affinity of the solvent to the polymer components. For a given system, a solvent that is good for one block can be classified as neutral, slightly selective, or strongly selective according to whether it is good, near Θ conditions, where Θ is the average radius of giration in solution, identical to the volume in the solid state, conditions, or a nonsolvent for the other block. Chloroform has a pronounced selectivity for PS, while toluene dissolves both segments of the tri-block copolymer very well.

2.2. Morphology

In **Figure 3–5**, the AFM phase images (at the air interface) and the TEM images of the SBS membranes in **Table 3** are reported.

The definition of all notation used to label the samples is reported in the Experimental Section (see Table 6).

28Tl shows in-plane PS cylinders, i.e., the axes of which lie in the membrane plane (Figure 3). In particular, TEM characterization indicates the co-existence of two types of nanostructures: cylinders parallel to the surface and a gyroid structure as reported by Khandpur et al.[32] The pitch of the PS columns for the 28Tl sample is of about 33 nm.

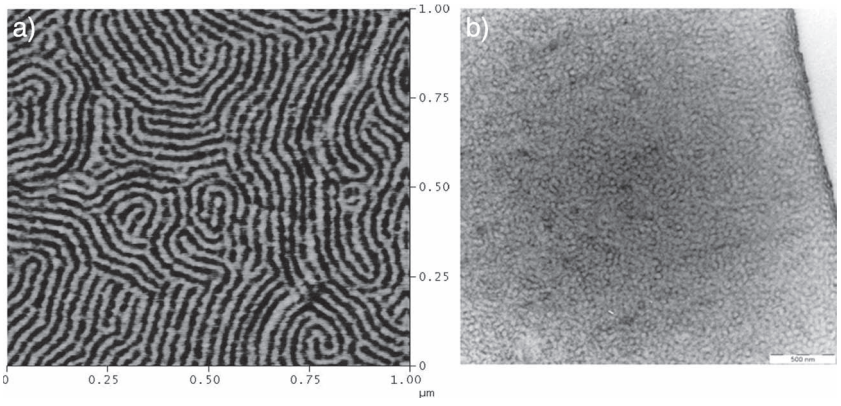

Figure 3. AFM phase image (a) and TEM cross section (b) of the top layer of the 28Tl sample.

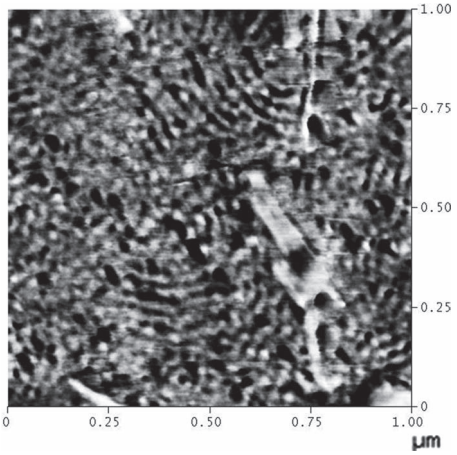

Figure 4. AFM phase image of the bottom layer of the 28Tl sample.

The bottom surface of the 28Tl sample shows PS cylinders parallel to the membrane surface, indicating that the phase separation, which starts at the film/air interface, is completed (**Figure 4**).

In perhaps the most commonly studied copolymer system, polystyrene-polybutadiene diblocks, the various equilibrium morphologies as a function of composition of the blocks are fairly well established.[33] A minor component compositions (PS) ranging from 0 to 20 wt% lead to spheres of the minor phase ordered in a cubic lattice in a continuous major-phase matrix (PB). Minor-component compositions ranging from 20 to 35 wt% cause minor phase cylinders (PS) arranged on a hexagonal lattice in a continuous major-phase matrix. Minor-component compositions greater than 35 wt% lead to a morphology of alternating lamellae. Therefore, the morphology of the 28Tl sample confirmed the morphology reported in the literature for similar systems. In particular, the morphology consisting of PS cylinders arranged with their axes aligned in the plane of the membrane is the one referred to as the equilibrium structure. On the basis of surface-energy consideration, PB block, which has a lower surface tension compared to PS and the glass substrate (**Table 4**) tend to occupy the film/air interface with in plane cylinder morphology. In fact, there is an extra energy associated with the cylinder ends in the vertical morphology: $\Delta G = 2\pi r^2 N_v \gamma_{PB/PS}$, N_v is the number of cylinders per unit volume, r is the cylinder radius, γ_i is the surface tension, and $\gamma_{PS/PB}$ is about 1.3 mJ m^{-2}.[21] However, under the conditions of casting of the films, the morphology can be influenced both by thermodynamic and kinetic factors. The diffusion of the solvent to the surface can play a controlling role in defining the morphology. In SBS triblock copolymers toluene diffusion in PS is much lower than that in PB. Kim and Libera [21] reported that the solvent mobility is related not only to the microdomain size but also to the tortuosity associated with the morphology and its relative orientation. Larger values of tortuosity correspond to a longer diffusion path. In the case of PS cylinders, both the vertical and the in-plane orientations provide a continuous path for solvent diffusion through the PB phase to the surface. However, a higher tortuosity can be expected in the in-plane orientation than in the vertical one because a less direct path through the PB phase to the surface is available from the film interior for the in-plane case.

Phase contrast AFM images of 2 μm × 2 μm and 1 μm × 1 μm areas 21Tl film (top and bottom) are shown in Figure 5A,C and Figure 5B,D, respectively. PS cylinders aligned both perpendicular to and in-plane to the membrane surface are present, as confirmed by the morphology of the bottom layer (Figure 5C and 3D, for 2 μm × 2 μm and 1 μm × 1 μm areas, respectively).

The rate of evaporation of toluene was the same for both the samples; the only difference was the amount of PS present in the SBS polymer (21 wt% and 28 wt% for 21Tl and 28Tl, respectively, see **Table 5** and the Experimental Section). Toluene as a solvent is slightly more selective towards PS than PB (Table 2). Therefore, during the formation of the membrane surface, the preferential affinity for the PS blocks causes the earlier precipitation of the PB blocks while the PS ones are pushed towards the free surface. The tendency of the PB blocks to occupy the film/air interface (in-plane orientation of PS cylinders) due to its lower surface tension is hindered by the higher affinity of

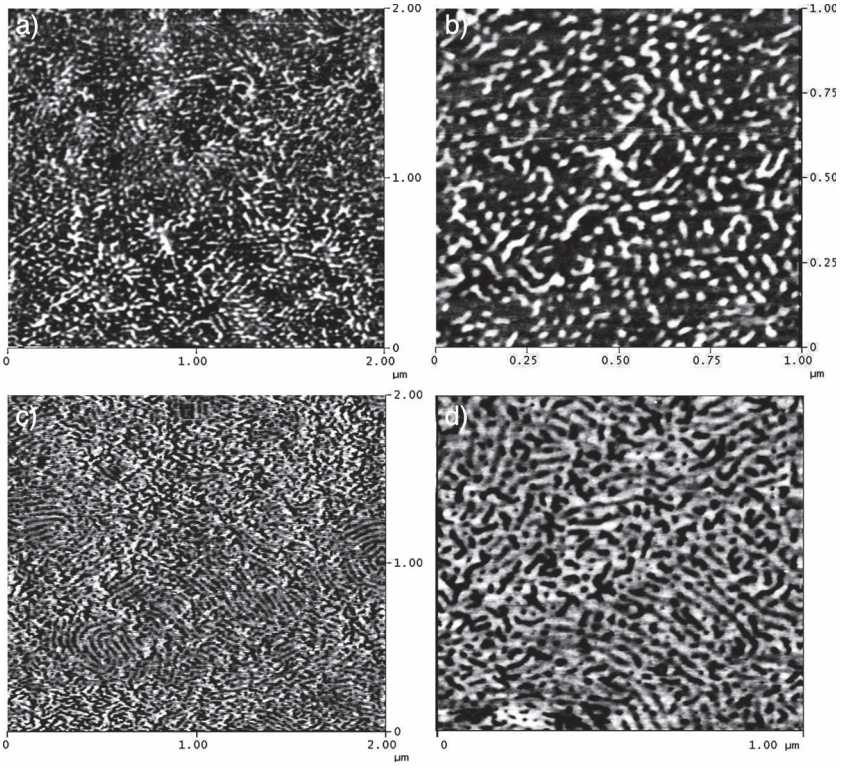

Figure 5. AFM phase images of Tl21: A,B) top layer and C,D) bottom layer for 2 μm × 2 μm and 1 μm × 1 μm areas, respectively.

Table 3. Morphology, swelling ability, and transport properties of SBS membranes. The normalized permeability is obtained by dividing the measured permeability by the weight fraction of the polybutadiene phase. Permeability in barrer (1 Barrer ≡ 10^{-10} cm^3 (STP) cm cm^{-2} cm Hg^{-1} s^{-1}).

Entry	Film	Thickness[a)] [μm]	Membrane morphology	Swelling in ethanol [wt%]	Permeability (normalized permeability)			Ideal selectivity [-]	
					CO_2	N_2	CH_4	CO_2/N_2	CH_4/N_2
1	28Tl	66.0 ± 1.4	In plane PS cylinders, 33 nm pitch	1.36	264 (367)	13 (18)	48 (67)	20,0 ± 0.94	3.7 ± 0.18
2	21Ch	120.0 ± 1.6	Disordered in plane PS cylinders, 42 nm pitch	1.14	237 (300)	7.9 (10)	33 (42)	30.0 ± 1.4	4.1 ± 0.19
3	28Ch	69.8 ± 1.5	Perpendicular PS cylinders	7.11	286 (397)	7.0 (9.7)	36 (50)	41 ± 1.9	5.1 ± 0.24
4	21Tl	70.0 ± 1.6	Perpendicular PS cylinders	14.7	289 (366)	5.8 (7.3)	41 (52)	50 ± 2.4	7.2 ± 0.34

[a)]The standard deviation of the measurements is reported.

the PS block chains for the solvent. This phenomenon occurs for the sample 21Tl, for which the PB content (79 wt%) is higher than that present in 28Tl (72 wt%).

In **Figure 6–9**, the morphological characterization of SBS films based on SBS21 and SBS28, respectively, prepared by using chloroform is given.

PS cylinders parallel to the membrane surface characterize sample 21Ch (Figure 6). It should be noted that the areal density of the PS cylinders, i.e., the total number of cylindrical domains on the surface, decreased in comparison to film 28Tl (Figure 3). The pitch increased from 33 nm to 42 nm. These differences compared to 28Tl sample arise from the lower PS content in the SBS 21 polymer. The membrane bottom layer shows two types of morphologies (Figure 7a,b): one is composed of PS cylinders in plane with the membrane (the same morphology of the top) while a disordered structure characterizes the second one, indicating that a non -omplete phase separation occurs.

For sample 28Ch, alignment of PS cylinders perpendicular to the surface occurs (Figure 8) near the skin layer. This is confirmed by TEM of the membrane cross section and by the analysis of the bottom surface, which shows only one type of morphology, indicating complete phase separation (Figure 9).

In copolymers containing two highly immiscible blocks, the solvent mediates non-favorable interactions between the segments forcing the copolymer to disorder. As the solvent evaporates, the concentration of solvent at the surface is lowest and a gradient in solvent concentration develops normal to the surface. With time, the concentration of solvent at the surface decreases and a microphase separation occurs only at the surface. The copolymer within the film is still disordered due to the higher concentration of solvent. Further solvent evaporation causes an ordering front to propagate through the film. In this context, solvent diffusion plays a crucial role on morphological orientation and can be considered in terms of the solvent concentration gradient within the film.

Chloroform has a pronounced affinity for PS blocks compared to PB blocks (χ_{PS} = 0.34 and χ_{PB} = 0.47, Table 2) while toluene, as above reported, is slightly selective for PS (χ_{PS} = 0.34 and χ_{PB} = 0.40, respectively, Table 2). Immediately cast solution of SBS 28 in $CHCl_3$ exhibits a higher concentration of PS block than the analogue solution based on SBS 21. Under such conditions, PS cylinders would grow in the direction of the maximum solvent concentration gradient and adopt an orientation perpendicular to the plane of the film (Figure 8,9).

Table 4. Surface energy of the substrate used for the membrane preparation and of the polymer blocks.

	Glass	Polystyrene	Polybutadiene
Surface energy [10^{-3} N m^{-1}]	100[34]	36[35]	32.5[36]

Table 5. Summary of the experimental conditions for the preparation of the SBS membranes.

Membrane code	Polymer, PS [%]	Solvent	Polymer in the solution [wt%]
28Tl	SBS28	toluene	20
28Ch	SBS28	chloroform	11
21Tl	SBS21	toluene	20
21Ch	SBS21	chloroform	11

2.3. Gas Transport

In Table 3 the morphology, the swelling ability and the gas transport characterization of SBS membranes are reported. If we consider that the gas permeability of glassy polystyrene is negligible with respect to the rubbery polybutadiene and that the density of the two polymers is very close, it is possible to work out the permeability of the PB fraction by dividing the experimental permeability by the weight fraction of the polybutadiene phase. This value is reported in Table 3 as the normalized permeability

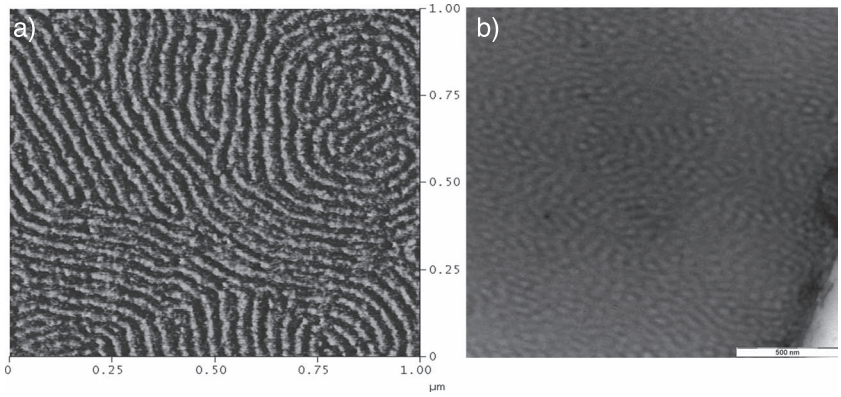

Figure 6. AFM phase image (left) and cross section TEM (right) of the top layer of the 21Ch sample

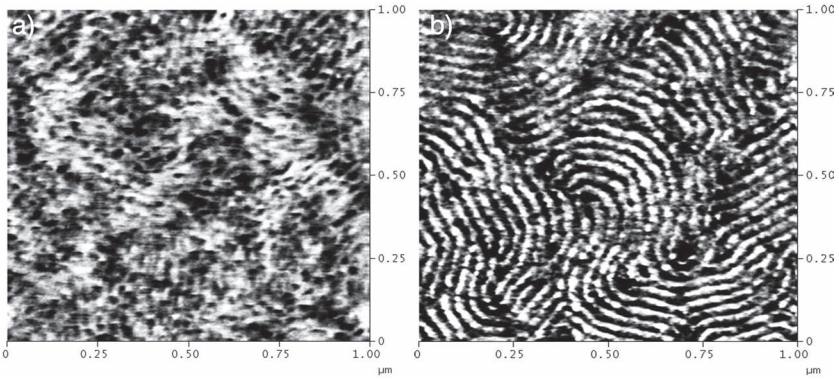

Figure 7. AFM phase image of two different portions of the bottom layer of the 21Ch sample.

(in parentheses). Based on the data in Table 3, all of the samples show very good separation performance. In particular, the selectivities for the CH_4/N_2 pair for the samples 28Ch and 21Tl, with values of 5.1 and 7.2, respectively, are higher than the values of the existing polymers used for this separation (Table 1) and are associated with a structure made of an hexagonal array of long PS cylinders normal to the membrane surface.

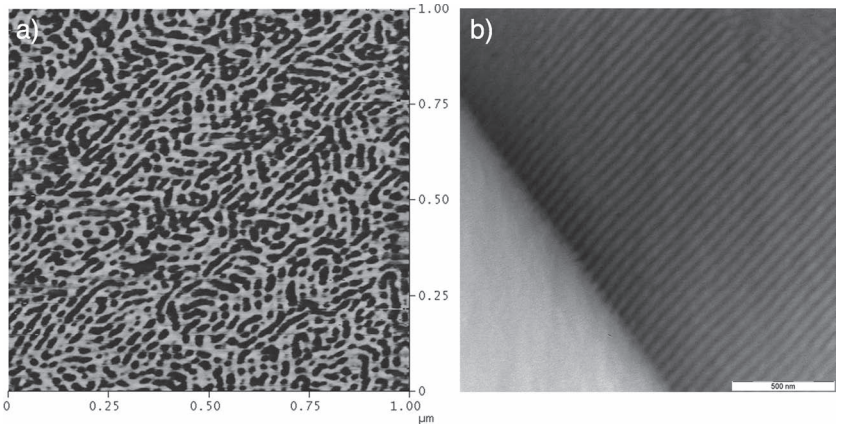

Figure 8. AFM phase image (a) and cross section TEM (b) of the 28Ch top layer.

Samples 28Tl and 21Ch (entries 1 and 2, Table 3) with the lower selectivity among the four SBS samples for CH_4/N_2 (3.7 and 4.1, respectively) and CO_2/N_2 (20 and 30, respectively) are characterized by the presence of well-defined PS cylinders in plane to the membrane surface. As reported above, the difference between these two samples concerns the areal density of PS cylinders (lower for 21Ch than 28Tl) and their pitches (42 nm and 33 nm for 21Ch and 28Tl, respectively).

It is noteworthy that both samples 28Ch and 21Tl (entries 3 and 4, Table 3) show an increase of the normalized CO_2 permeability (397 Barrer and 366 Barrer, respectively) compared to 28Tl and 21Ch and better selectivity for both CO_2/N_2 and CH_4/N_2 due to the decrease of N_2 permeability (9.7 and 7.3 Barrer, respectively).

SBS membranes show the typical behavior of rubbery polymers, characterized by higher permeability for CO_2 than for permanent gases.[27,28] In rubbery polymers the solubility of CO_2 is higher than for permanent gases, but the mobility of the polymer chains reduces the ability to sieve penetrant molecules on the basis of size. In SBS the permeable amorphous rubbery phase (PB) is responsible for the permeation, whereas the glassy (PS) phase cross-links the PB phase. It is evident from the data in Table 5 that the amount of permeable polymer (PB) alone cannot account for the differences in the transport of gas among the SBS membranes. Other criteria for the interpretation of the experimental data that will be considered in the following are membrane morphology, swelling ability, and tortuosity.

The swelling ability of SBS is influenced by the microphase morphology of the SBS polymers. Aligned PS cylinders enable SBS to swell with less hindrance along the plane normal to the direction of their axes, but they represent rigid elements that reduce swelling in the direction parallel to their axes. Instead, curved PS cylinders do not enable a comparable swelling of the PB phase because non-parallel adjacent PS cylinder segments hinder the swelling of the PB phase along the direction parallel to their axis. This situation can be easily visualized by considering a simplified system consisting of two cubic SBS domains (**Figure 10**) that share one face on the *y*–*z* plane and in which the direction of the parallel PS cylinders is orthogonal: along the direction of the *y*-axis in the left cube and along the direction of the *z*-axis in the cube to the right in Figure 10. When a strongly absorbing species is present, the left cube tends to swell in the *x*–*z* plane,

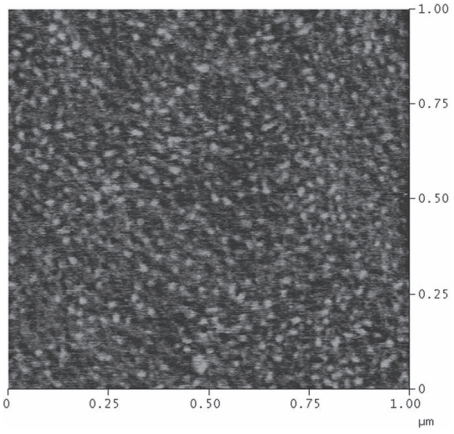

Figure 9. AFM phase image of the 28Ch bottom layer.

the right cube in the *x*–*y* plane. Unfortunately, the left cube hinders the swelling of the right cube along the *y*-direction and the right cube instead hinders the swelling of the left cube along the *z*-direction. In other words, the different orientation of the PS phases reduces the tendency to swell and also the sorption ability of the PB phase. If the right cube in Figure 10 is surrounded by six similar cubes with orthogonal orientations of the PS cylinders, the swelling ability of the SBS domain would be greatly depressed on the two faces normal to the PS cylinders, and the cube would limit the swelling of four neighbour cubes sharing the faces parallel to the PS cylinders. For what concerns the two samples prepared from toluene, the swelling in ethanol of the 28Tl sample, with a tortuous arrangement of the curved PS cylinders, is just 1.36% and represents the 9.3% swelling of the 21Tl sample (14.7%) with a parallel arrangement of straight PS cylinders. This trend is confirmed by the samples prepared in chloroform: the swelling of 28Ch with a perpendicular arrangement is of 7.11% while that observed for 21Ch with PS cylinders parallel to membrane surface is 1.14%.

It is speculated that the unusually high CH_4/N_2 ideal selectivity observed for the SBS films with aligned columnar PS cylinders stems from a very high solubility selectivity in favor of CH_4 because the molecule CH_4 is larger than N_2 (kinetic diameters 0.38 and 0.364 nm, respectively[37]). This means that N_2 diffuses faster than CH_4. This hypothesis is supported by the correlation between the CH_4/N_2 ideal selectivity of the four membranes studied and their swelling ability in ethanol (Table 3). In fact, a modest swelling ability limits the sorption of gas and therefore should depress the sorption selectivity in favor of methane. Similar arguments are able to rationalize the high CO_2/N_2 ideal selectivity of 40 and 50 observed for the same SBS films.

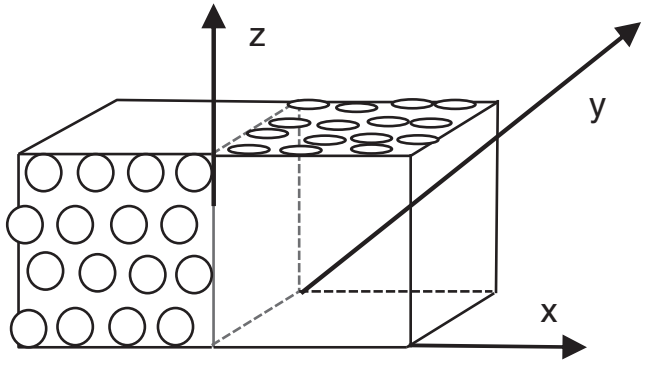

Figure 10. Schematic representation of two SBS cubes sharing one face with orthogonal orientation of linear rigid PS cylinders.

For CO_2, the effect of the swelling ability seems relevant in that the two membranes with the aligned columnar structure (28Ch and 21Tl) display a higher normalized permeability than the corresponding membranes with curved PS cylinders (28Tl and 21Ch). The lowest CO_2 normalized permeability of sample Ch21 might be an indication that the disordered arrangement of the in-plane PS cylinders crosslinks in a more effective way the polybutadiene phase and interferes with swelling. On the other hand, the relatively high CO_2 normalized permeability of sample 28Tl (367 Barrer) with in-plane PS cylinders and the modest ethanol swelling (1.36%) indicate that, under the conditions used in the permeation experiments, the swelling induced by CO_2 is modest.

Pure N_2 is not strongly absorbed by SBS, its swelling ability is modest, and, therefore, the arguments invoked for the rationalization of the trend of CO_2 permeability may not be valid in this case. Indeed, no straightforward explanation can be given for the fact that the largest normalized N_2 permeability (18 Barrer) corresponds to the 28Tl sample with only 1.36% swelling in ethanol, whereas the smallest normalized N_2 permeability (7.3 Barrer) is found through the 21Tl sample with 14.7 wt% swelling. Tortuosity can hardly be invoked because a higher tortuosity has to be expected in the in-plane morphology rather than in the vertical morphology. A less direct path through the PB phase is available from the film interior for the in-plane case; therefore the normalized length of the path that a molecule has to travel to cross the membrane (tortuosity) should be lowest for the two less N_2 permeable membranes (21Tl and 28Ch), which display a morphology of straight PS cylinders normal to the membrane surface.

3. Conclusions

New nanostructured gas separation membranes were successfully prepared by using SBS triblock copolymers containing 28 wt% styrene and, for the first time in the literature, 21 wt% styrene. Both characteristic types of morphology, i.e., PS (hard minority block) cylinders in plane of PB (soft majority block) and PS cylinders perpendicular to the membrane surface, have been obtained by varying the membrane preparation conditions. The gas transport characterization indicates that the most appropriate polymer-solvent combinations are SBS 28% and chloroform (11 wt%) (sample 28Ch) and SBS 21% and toluene (20 wt%) (sample 21Tl). In particular, for this last sample outstanding performance in terms of selectivity and permeability for CH_4/N_2 and CO_2/N_2 gas pairs has been observed. High selectivity corresponds to high swelling ability and is related to a membrane morphology in which PS columns are normal to the membrane surface.

Comparison of the gas separation performance with block co-polymer membranes described in the literature showed the

Table 6. Characteristics of the SBS solvents used here.[31]

	Solubility parameter δ [$J^{1/2}$ $cm^{-3/2}$]	Molar volume V [mL mol^{-1}]	Boiling point (T_b) [°C]	Evaporation rate	Vapor pressure at 30 °C [mmHg]
toluene	18.2	106.8	111	2.24	36.7
chloroform	19.0	80.7	61	11.60	209

advantage of the well-defined SBS morphology. The present work clearly shows that the solvent evaporation method with the appropriate membrane preparation conditions (percentage of PS, polymer concentration, type of solvent) offers a versatile tool to tailor mass transfer and separation properties of membranes for gas separation of high industrial interest.

4. Experimental Section

Materials: Styrene-butadiene-styrene block co-polymers (28 wt% and 21 wt% polystyrene) were purchased from Sigma-Aldrich. Toluene (VWR) and chloroform (Carlo Erba) were reagent grade and used without purification. The characteristics of the two solvents are listed in **Table 6**.

Membranes: A predetermined amount of polymer was dissolved in the organic solvent with magnetic stirring overnight at 25 °C to make 11 and 20 wt% solutions. Each solution was poured into a steel ring on a levelled glass surface. The ring was covered to slow down the evaporation of the solvent. The resulting membranes were dried under vacuum at 40 °C to remove the residual solvent. The thickness of the membranes has been measured with a micrometer (Carl Mahr, Germany) in several points, and the average value has been considered for the determination of the permeability.

In Table 4 the surface energy of the substrate used for the membrane preparation and of the block copolymers are reported.

In Table 5, a summary of the experimental conditions for the preparation of the membranes is given.

Membrane Swelling: Dry strips of membranes were submersed in pure ethanol in closed vials at room temperature. After 24 h of equilibration, the strips were taken out of the vials, wiped to remove the excess liquid on the surface and weighed immediately. Membrane uptake was calculated using the equation:

$$\%\text{sorption} = \frac{W_s - W_d}{W_d} \times 100 \quad (5)$$

where W_s is the mass of the swollen membrane and W_d is the mass of the dry membrane.

AFM Characterization: AFM was used to image the surface morphology in the tapping mode. In this method, the cantilever oscillates up and down close to its resonance frequency so that the tip is in contact with the sample surface periodically. When the tip is brought close to the surface, the vibration of the cantilever changes due to the tip–sample interaction. Recent developments of the tapping mode AFM allow the detection of shifts in the phase angle of vibration when the oscillating tip interacts with the sample surface. The phase shift provides information on other surface properties such as stiffness, viscoelasticity, and adhesion. A Nanoscope IIIa (Veeco, CA) was used for the AFM characterization of the different membranes in air. Silicon probes with resonance frequency 200–400 kHz, nominal tip radius of curvature 10 nm, and cantilever length 125 μm were used.

Surface roughness was estimated from topography images acquired in different areas of the single membranes. Phase images were acquired simultaneously with the topography. Materials with different viscoelasticity were clearly distinguishable. The softer domains appeared dark (PB) while the stiffer ones appeared bright (PS) in the phase images.

TEM: For routine TEM, specimens were fixed in 3% osmium tetroxide solution in 0.1 M phosphate buffer (pH. 7.4) for 12 h at 4 °C. Infiltration was carried out overnight using pure LR White acrylic resin (London Resin Co., Berkshire, UK). The samples were embedded in fresh LR White in gelatin capsules and polymerized for 24 h at 50 °C. Ultrathin sections were prepared using a diamond knife and collected on copper grids, vapor stained with osmium tetroxide, and then examined with a Zeiss EM 10 electron microscope.

Gas Permeability Measurements: The pure gas permeance of the SBS membranes was measured at 25 °C and 1 bar of feed pressure gradient by means of a volumetric apparatus schematized in Figure S1 (Supporting Information). The apparatus allowed the evacuation of the upstream and of the downstream side of the membrane and was protected from the back-diffusion of oil with a liquid nitrogen trap. Prior to each measurement the membranes were evacuated for about 30 min to guarantee the complete removal of dissolved gases or vapors from the membrane and from the sealing rings. Then the permeating gas was carefully introduced at atmospheric pressure on both sides of the membranes and afterwards the pressure was increased on the feed side to start the permeation measurements. The permeability reported in this work refer to the steady state, i.e., at the time when permeability becomes constant in time. The error affecting the permeability values obtained with the device used in this work is estimated to be 6.1–9.0% (see Supporting Information, Table S1). The error in the determination of membrane thickness affects all permeability values to the same extent and, therefore, does not propagate to selectivity, which is calculated as a ratio of permeability values on the same membrane, the error of which is evaluated to 4.7% (see Supporting Information).

Supporting Information

Supporting Information is available from the Wiley Online Library or from the author.

Received: August 14, 2011
Revised: December 23, 2011
Published online: February 10, 2012

[1] K. Lokhandwala, I. Pinnau, Z. He, K. D. Amo, A. DaCosta, J. G. Wijmans, R. W. Baker, *J. Membr. Sci.* **2010**, *346*, 270.
[2] R. W. Baker, K. Lokhandwala, *Ind. Eng. Chem. Res.* **2008**, *47*, 2109.
[3] S. A. Stern, V. M. Shah, B. J. Hardy, *J. Polym.Sci: Polym. Phys. Ed.* **1987**, *25*, 1263
[4] A. Car, C. Stropnik, W. Yave, K.-V. Peinemann, *J. Membr. Sci.* **2008**, *307*, 88.
[5] S. R. Reijerkerk, A. Arunb, R. J. Gaymans, K. Nijmeijer, M. Wessling, *J. Membr. Sci.* **2010**, *359*, 54.
[6] L. A. Utracki, *Polym. Eng. Sci.* **1995**, *35*, 2.
[7] V. Bondar, B. D. Freeman, I. Pinnau, *J. Polym. Sci. Part B Polym. Phys.* **1999**, *37*, 2463.
[8] J. H. Kim, S. Y. Ha, Y. M. Lee, *J. Membr. Sci.* **2001**, *190*, 179.
[9] J. C. Chen, X. Feng, A. Penlidis, *Sep. Sci. Technol.* **2004**, *39*, 149.
[10] H. Lin, B. D. Freeman, *J. Mol. Struct.* **2005**, *739*, 57.
[11] V. Barbi, S. S. Funari, R. Gehrke, N. Scharnagl, N. Stribe, *Macromolecules* **2003**, *36*, 749.
[12] M. Yoshino, K. Ito, H. Kita, K.-I. Okamoto, *J. Polym. Sci. B: Polym. Phys.* **2000**, *38*, 1707.
[13] C. Damian, E. Espuche, M. Escoubes, S. Cuney, P. J. Pascault, *J. Appl. Polym. Sci.* **1997**, *65*, 2579.

[14] S. J. Metz, M. H. V. Mulder, M. Wessling, *Macromolecules* **2004**, *37*, 4590.
[15] H. B. Park, C. K. Kim, Y. M. Lee, *J. Membr. Sci.* **2002**, *204*, 257.
[16] D. Husken, J. Feijen, R. J. Gaymans, *Macromol. Chem. Phys.* **2008**, *209*, 525.
[17] Y. Thomann, R. Thomann, A. Hasenhindl, R. Mülhaupt, *Macromolecules* **2009**, *42*, 5684.
[18] H. Huang, Z. Hu, Y. Chen, F. Zhang, Y. Gong, T. He, C. Wu, *Macromolecules* **2004**, *37*, 6523.
[19] Q. Zhang, O. K. C. Tsui, B. Du, F. Zhang, T. Tang, T. He, *Macromolecules* **2000**, *33*, 9561.
[20] H. Huang, F. Zhang, Z. Hu, B. Du, T. He, F. K. Lee, Y. Wang, O. K. C. Tsui, *Macromolecules* **2003**, *36*, 4084.
[21] G. Kim, M. Libera, *Macromolecules* **1998**, *31*, 2569.
[22] J. M. Yang, G. H. Hsiue, H. L. Chen, *Polym. Eng. Sci.* **1996**, *36*, 425.
[23] S. G. Desai, S. K. Sikdar, *Clean Prod. Processes* **2000**, *2*, 140.
[24] S. Chovau, A. Dobrak, A. Figoli, F. Galiano, S. Simone, E. Drioli, S.K. Sikdar, B. Van der Bruggen, *Chem. Eng. J.* **2010**, *159*, 37.
[25] A. Dobrak, A. Figoli, S. Chovau, F. Galiano, S. Simone, I. F. J. Vankelecom, E. Drioli, B. Van der Bruggen, *J. Colloid Interface Sci.* **2010**, *346*, 254.
[26] A. K. Jha, L. Chen, R. D. Offeman, N. P. Balsara, *J. Membr. Sci.* **2011**, *373*, 112.
[27] F. Bazzarelli, P. Bernardo, F. Tasselli, G. Clarizia, V. G. Dzyubenko, P. Vdovin, J. C. Jansen, *Sep. Purif. Technol.* **2011**, *80*, 635.
[28] K. W. Song, K. R. Ka, C. K. Kim, *Ind. Eng. Chem. Res.* **2010**, *49*, 6587.
[29] J. Kim, P. Kim, H. Lee, *J. Appl. Polym. Sci.* **1996**, *66*, 1117.
[30] A. M. Peters, R. G. H. Lammertink, M. Wessling, *J. Membr. Sci.* **2008**, *320*, 173.
[31] D. W. van Krevelen, K. te Nijenhuis, *Properties of polymers*, 4th ed., Elsevier, Amsterdam **2009**.
[32] A. K. Khandpur, S. Forster, F. S. Bates, I. W. Hamley, A. J. Ryan, W. Bras, K. Almdal, K. Mortensen, *Macromolecules* **1995**, *28*, 8796.
[33] L. Leibler, *Macromolecules* **1980**, *13*, 1602.
[34] A. N. Kensington, *The Physics and Chemistry of Surfaces*, Oxford University Press, Oxford, UK **1941**.
[35] L. H. Lee, *J. Polym. Sci.* **1967**, *5*, 1103.
[36] E. A. Grulke, in *Polymer Handbook*, (Eds: J. Brandrup, E. H. Immergut), John Wiley & Son, New York **1989**.
[37] S. Wu, Polym. Eng. Sci. **1987**, *25*, 335.
[38] D. W. Breck, *Zeolite Molecular Sieves. Structure, Chemistry and Use*, John Wiley & Sons, New York **1974**.